RSC Advances

ROYAL SOCIETY OF CHEMISTRY

www.rsc.org/advances

Facile fabrication and electrochemical properties of high-quality reduced graphene oxide/cobalt sulfide composite as anode material for lithium-ion batteries

Zhangpeng Li,[a] Wenyue Li,[a,b] Hongtao Xue,[a] Wenpei Kang,[a] Xia Yang,[a] Mingliang Sun,[a] Yongbing Tang*[a,b] and Chun-Sing Lee*[a]

[a] Center of Super-Diamond and Advanced Films (COSDAF), Department of Physics and Materials Science, City University of Hong Kong, Kowloon, Hong Kong SAR, People's Republic of China.

[b] Functional Thin Films Research Center, Shenzhen Institutes of Advanced Technology, Chinese Academy of Sciences, Shenzhen, People's Republic of China.

E-mail: ybtang@cityu.edu.hk; apcslee@cityu.edu.hk; Tel: +852-34427826

Abstract

A reduced graphene oxide (rGO)/cobalt sulfide composite is synthesized with a simple and efficient ultrasound-assisted wet chemical method. Morphology and microstructure of the composite are examined with field emission scanning electron microscopy, transmission electron microscopy, X-ray diffraction, Raman spectroscopy, and X-ray photoelectron spectroscopy. The results confirm that cobalt sulfide nanoparticles are homogeneously and tightly attached on the surfaces of rGO. As an anode material for lithium-ion batteries, this composite delivers a high reversible capacity of 994 mAh g^{-1} after 150 cycles at a current density of 200 mA g^{-1}. A synergistic effect combining the merits of rGO and cobalt sulfide nanoparticles endow the composite with superior electrochemical performances over those of pure cobalt sulfide.

Keywords: Cobalt sulfide; Graphene; Composite; Anode; Lithium ion battery

1. Introduction

Lithium-ion batteries (LIBs) with high storage capacity and good cycling stability are of increasing demand for applications in portable electronic devices and hybrid electric vehicles [1-3]. In commercial LIBs, graphite is commonly employed as the anode material because of its flat potential profile *versus* lithium and its structural stability during cycling. However, the small theoretical capacity of graphite (372 mAh g^{-1}) necessitates the development of alternative anode materials [4, 5]. Unlike graphite materials, inorganic nanomaterials, including metal oxides [6-9], nitrides [10, 11], and chalcogenides [12-15], are based on unusual conversion reaction mechanisms and some of them show high reversible capacities. Among these materials, cobalt sulfides in the form of various crystalline phases with a wide range of stoichiometries, including CoS, CoS_2, Co_3S_4, and Co_9S_8, and nonstoichiometric $Co_{1-x}S$ have attracted much attention due to their high theoretical capacity, good thermal stability, natural abundance and environment friendliness [16-18]. However, like other conversion reaction-based anode materials, there are still many challenges on practical LIB application of cobalt sulfide. These include their poor rate capability, limited capacity and rapid capacity fading, caused by their low conductivity and drastic volume expansion during the discharge/charge process. In general, two widely used strategies have been developed to address these problems. One approach is to accommodate the volumes change with novel nanostructures [19-21]. The other effective way is to introduce carbonaceous materials, because the elastic feature of carbon supports can provide a cushion effect against volume strain. Meanwhile, the carbon materials can

also improve the electrical conductivity of the cobalt sulfide anode materials [22-24]. As a versatile carbonaceous material, graphene is an excellent substrate for loading active nanomaterials for LIBs due to its outstanding electronic conductivity, high charge mobilities, good mechanical strength, structural stability and large specific surface areas [25-27]. It has been reported that the Li-storage performance of cobalt sulfide could be improved by combining with graphene [28-31]. For example, compared to pure CoS_2 with fast capacity fading after 10 cycles, a CoS_2/graphene composite retains a reversible capacity of 650 mAh g^{-1} after 40 cycles at 50 mA g^{-1} [28]. In another work, a solvothermal method was reported to synthesize cobalt sulfides/graphene composite. LIB anode made from this composite still have a reversible capacity of 950 mAh g^{-1} after 50 cycles at a current density of 100 mA g^{-1} [29]. Namely, graphene is able to increase the conductivity of cobalt sulfide and cushion its volume change stress during charge/discharge process. It is noteworthy that although remarkable progresses have been made, challenges such as the time consuming synthesis methods, poor connection between graphene and the cobalt sulfide materials, and low production rate, etc., still need to be addressed.

Here, a reduced graphene oxide (rGO)/cobalt sulfide composite was synthesized by a simple and efficient ultrasonic-assisted wet chemical method at low temperature. Cobalt sulfide nanoparticles are found to be tightly and homogeneously attached onto the surface of rGO forming an ultrathin sheet like structure. The composite shows excellent lithium storage properties with high capacity (about 994 mAh g^{-1} after 150 discharge/charge cycles at a current density of 200 mA g^{-1}) and good rate capability.

2. Experimental

2.1 Synthesis of rGO/cobalt sulfide

Graphene oxide (GO) was synthesized from natural graphite powder using a modified Hummers' method (see the Supporting Information) [32, 33]. The rGO/cobalt sulfide composite was prepared with a simple and efficient route. In a typical process, 160 mL GO aqueous dispersion (0.25 mg mL^{-1}) was mixed with 35 μL hydrazine hydrate (80%) and 625 μL $NH_3 \cdot H_2O$ (25%) via sonication. 2 mmol $Co(CH_3COO)_2 \cdot 4H_2O$ was dissolved in 40 mL deionized water and slowly added into the above homogeneous GO solution and then sonicated for another hour. Subsequently, freshly prepared Na_2S solution (1.0 g in 1 mL deionized water) was added dropwise under sonication. All reactions were carried out without external heating and the temperature during reactions is in the range of 45 to 50 ^oC. After 1 hour ultrasonic assisted reaction, the composite was filtrated, washed with deionized water and freeze-dried. Finally, the product was annealed in Ar/H_2 (95/5 *v*/*v*) gas at 400 ^oC for 2 hours. For comparison, pure cobalt sulfide was also prepared by a similar procedure in the absence of GO.

2.2 Characterization

Morphologies, structures, and chemical compositions of the samples were investigated with scanning electron microscopy (SEM, Philips FEG SEM XL30) and energy-dispersion X-ray spectroscopy (EDX), transmission electron microscopy (TEM, Philips CM200 FEG TEM operated at 200 kV), atomic force microscopy (AFM, VEECO Nanoscope IIIa), X-ray diffraction (XRD, Philips X'Pert

diffractometer with Cu Kα radiation), Raman spectroscopy (Renishaw 2000 laser Raman microscope equipped with a 514 nm argon ion laser), and X-ray photoelectron spectroscopy (XPS, VG ESCALAB 220i-XL surface analysis system, using a monochromated Al Kα X-ray gun with photon energy of 1486.6 eV.)

2.3 Electrochemical Measurements

Electrochemical characterizations were measured with CR2032 coin-type cells assembled in a dry argon-filled glove box (MBRAUN, MB 200B) with an oxygen concentration below 1 ppm. The working electrodes were prepared by mixing the composite, carbon black, and sodium carboxylmethyl cellulose (CMC) with a weight ratio of 70:20:10 and pasting onto a copper foil. The test cell consists of a working electrode and a lithium counter electrode, which were separated by polypropylene membrane (Celgard 2400, Inc., USA). The electrolyte is a solution of 1 M $LiPF_6$ in ethylene carbonate (EC)/dimethyl carbonate (DMC) (1:1 in volume). Galvanostatic discharge/charge experiments were carried out with a MACCOR 4000 battery test system over a voltage window of 0.01-3.0 V (vs. Li^+/Li). Cycle voltammetry (CV) was measured using a CHI 660D electrochemical workstation. Electrochemical impedance spectroscopy (EIS) measurements were performed with a ZAHNER-elektrik IM6 impedance measurement unit over a frequency range of 0.01-10^5 Hz with an AC amplitude of 5 mV.

3. Results and Discussion

AFM morphological image and the corresponding cross-section analysis of GO on the silicon substrate demonstrate that the average thickness of GO sheets is

approximately 1 nm (Fig. S1 in Supporting Information), indicating single-layered GO sheets have been obtained [31, 34]. XRD pattern of sample obtained before adding Na_2S is shown in Fig. S2. The diffraction peaks can be indexed to $Co(OH)_2$ and CoOOH. As cobalt acetate salt is added to the GO dispersion, the Co^{2+} ions coordinate to the negatively charged GO layers and henceforth act as nucleation centers for the formation of $Co(OH)_2$ and CoOOH nanocrystals. After ultrasonically treat for 1 hour, $Co(OH)_2$ and CoOOH are uniformly formed on the surfaces of rGO (Fig. S2b). Upon addition of Na_2S, the $Co(OH)_2$ and CoOOH nanocrystals attached to the rGO layers are converted into cobalt sulfide nanocrystals [35]. Under this condition, the GO is simultaneously reduced to rGO. Finally, the product was annealing at 400 ^oC in Ar/H_2 (95:5 vol. ratio) for 2 hours to obtain the final composite material.

The crystalline phase of cobalt sulfide in the prepared composite was determined by XRD. As shown in Fig. 1a, the XRD pattern of the composites indicate that it contains mainly cubic Co_9S_8 (ICDD PDF #86-2273) belonging to the *Fm-3m* space group (no. 225). Additionally, diffraction peaks originated from $Co_{1-x}S$ (ICDD PDF #42-0826) can also be observed. For pure cobalt sulfide prepared in the absence of GO, all of the diffraction peaks can be indexed to the Co_9S_8 phase with relative poor crystallization.

It is well known that Raman spectroscopy is a powerful technique to study carbonaceous materials. Here, Raman spectroscopy is used to confirm the existence of rGO in the as-prepared composite. Fig. 1b shows typical Raman spectra of the pure

cobalt sulfide and the rGO/cobalt sulfide composite. Compared to the spectrum of pure cobalt sulfide, in the spectrum of the rGO/cobalt sulfide composite, two peaks at 1353 and 1584 cm^{-1} appear, corresponding to the breathing modes of rings or κ-point phonons of A_{1g} symmetry (D band) and the E_{2g} phonon of sp^2-bonded carbon atoms in a two-dimensional hexagonal lattice (G band), respectively, which suggests the existence of rGO.

XPS was used to provide further evidence for the successful combination of cobalt sulfide with rGO, and to examine chemical state of cobalt and sulfur in the composite. Fig. 1c shows a survey spectrum, indicating the composite consists of C, O, S and Co. A Co $2p_{2/3}$ core level spectrum is shown in Fig. 1d. The two main peaks at 778.4 and 781.0 eV can respectively be attributed to Co-S and Co-O bonds, respectively [36-38]. The Co-O bond was derived from the coordination between the unstable surface cobalt ions and oxygen atoms from the rGO [36, 39]. Besides, a shake-up satellite can be found at about 785.0 eV. The peaks between 790 and 805 eV are the corresponding Co $2p_{1/2}$ signals of their Co $2p_{3/2}$ counterparts. For the S_{2p} core level spectrum (Fig. 1e), the peaks located at 161.6 and 162.5 eV are attributed to sulfide (S^{2-}) and metal deficient sulfide (S_2^{2-}) species, respectively. The peaks at 163.3 and 164.3eV correspond to polysulfides (S_n^{2-}) [40-43].

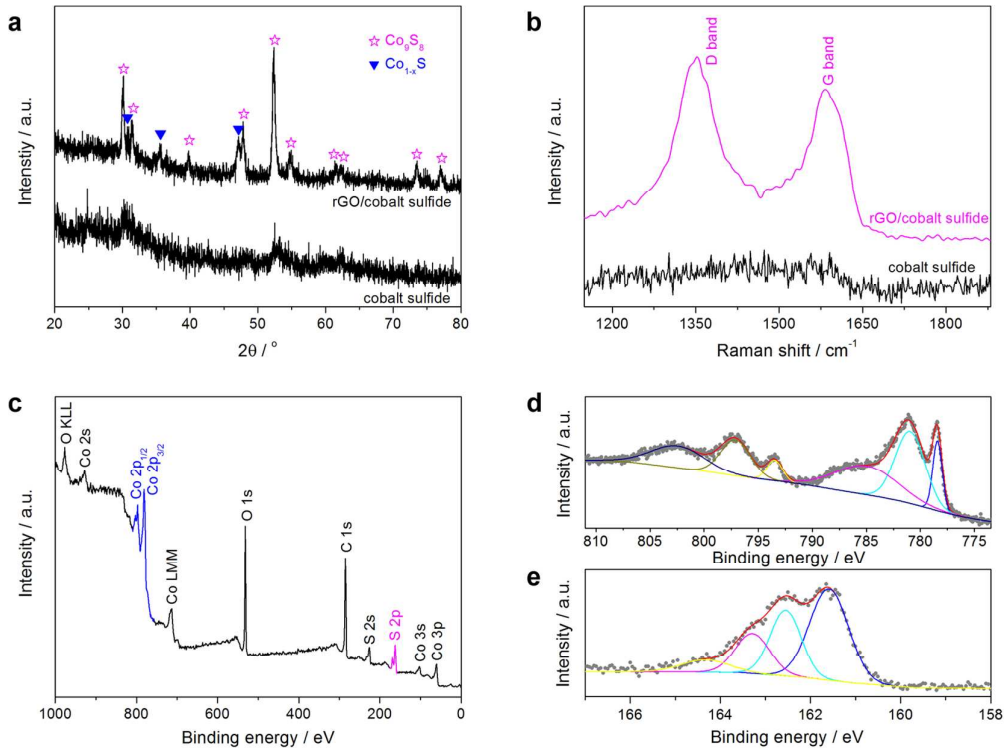

Fig. 1. (a) XRD pattern of the prepared pure cobalt sulfide and rGO/cobalt sulfide composite, (b) Raman spectrum of the pure cobalt sulfide and the rGO/cobalt sulfide composite, (c) XPS survey spectrum, (d) Co 2p and (e) S 2p core level spectra of the prepared rGO/cobalt sulfide composite.

Morphologies and microstructures of the as-prepared samples were investigated by SEM and TEM. Fig. 2a is an SEM image of the rGO showing characteristic wrinkled thin veil-like structure with many folds at the edges (The detailed characterization and analysis of the rGO are listed in Fig. S3 in Supporting Information.). For the rGO/cobalt sulfide composite, the morphology exhibits a loosely packed structure consisting of some sheet-like building units inheriting from rGO (Fig. 2b). Such a structure provides easy access of the electrolyte to the interfaces of the electrode

material. In contrast, the pure cobalt sulfide shows a more compact structure than that of the composite (Fig. S4 in Supporting Information), suggesting the introduction of rGO facilitates formation of loose structure.

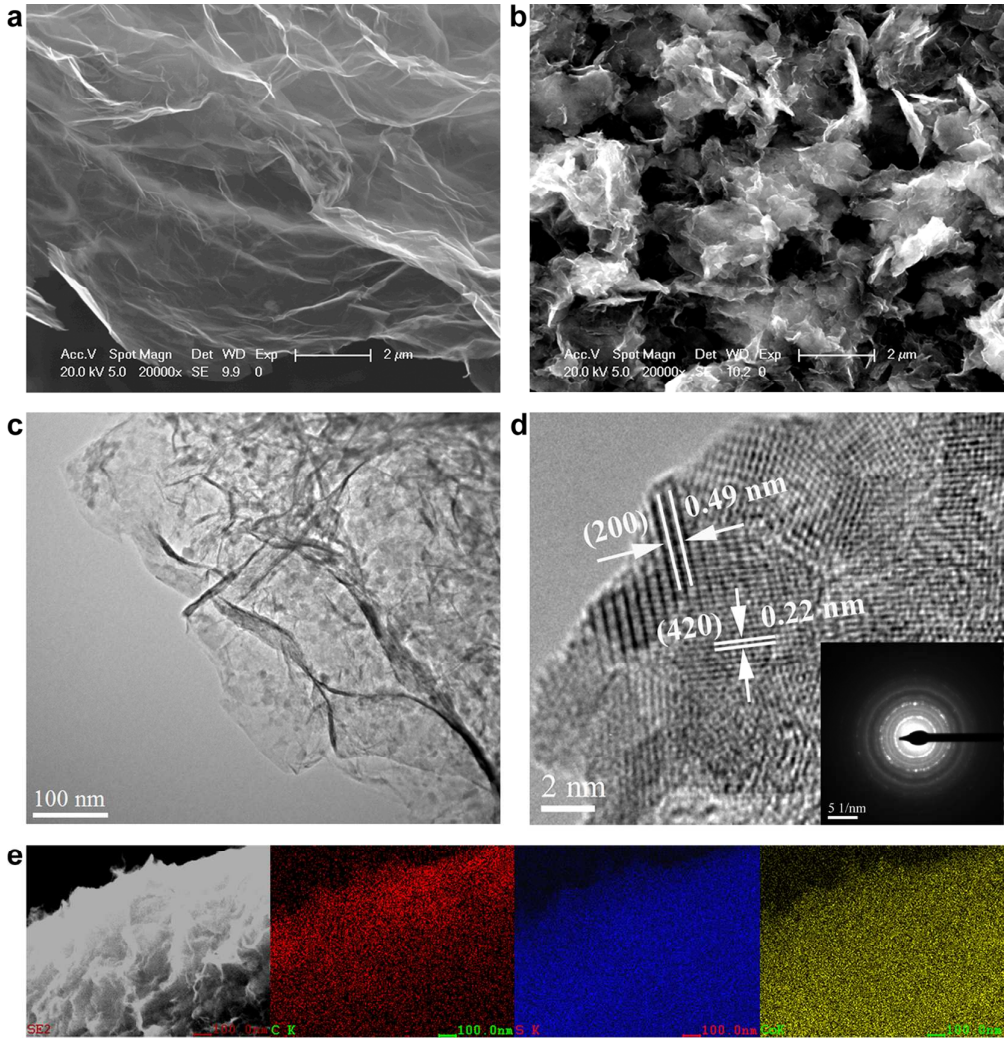

Fig. 2. SEM images of (a) rGO and (b) rGO/cobalt sulfide composite, (c) A TEM and (d) an HRTEM images of the rGO/cobalt sulfide composite, (e) an SAED pattern of the composite, and (f) EDS elemental mapping of the composite.

A TEM image (Fig. 2c) of the rGO/cobalt sulfide composite reveals that cobalt sulfide nanoparticles are uniformly attached on the rGO sheets. An HRTEM image

(Fig. 2d) shows lattice fringe spacings of about 0.49 and 0.22 nm, which correspond respectively to spacings of the (200) and the (420) planes of the Co_9S_8 phase. In addition, a corresponding SAED pattern of the composite (Fig. 2e) shows the polycrystalline nature of the Co_9S_8. The diffraction rings can be readily indexed to the (311), (400), (440), (511) and (800) planes of the Co_9S_8 phase, which is in a good agreement with the XRD analysis. Fig. 2f shows EDS mappings of the rGO/cobalt sulfide composite. It is clearly shown that the elements of C, S, and Co are homogenously distributed, indicating uniform coating of cobalt sulfide on the rGO surfaces.

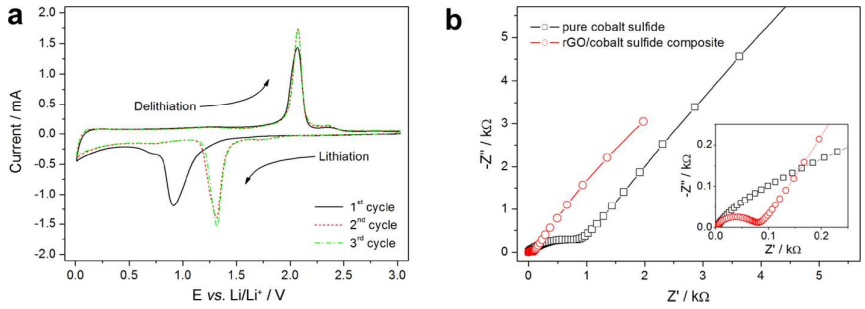

Fig. 3. (a) CV curves of the rGO/cobalt sulfide composite at a scan rate of 0.1 mV s^{-1} and (b) EIS of the rGO/cobalt sulfide composite and pure cobalt sulfide electrodes.

CV and EIS tests were performed with coin-type test cells to study the electrochemical reactions in the composite during the lithiation/delithiation processes. Fig. 3a shows typical CV curves of the prepared rGO/cobalt sulfide composite anode for the first three cycles over a voltage window of 0.01-3.0 V (vs. Li^+/Li) at a scanning rate of 0.1 mV s^{-1}. It can be seen that the CV profiles show typical

characteristics of cobalt sulfide based anodes [24, 28]. In the first cycle, a broad and weak cathodic peak at about 0.68 V is ascribed to the decomposition of electrolyte and the formation of solid electrolyte interface (SEI) layer. The sharp cathodic peak at 0.91 V corresponds to the reduction of Co ion to Co^0 ($Co_9S_8 + 16Li^+ + 16e^- \leftrightarrow 8Li_2S + 9Co$). Such a peak is also observed, although significantly shifts to 1.3 V in the subsequent cycles, which is in good agreement with the literature [24, 44]. The lithiation voltage in the following cycles is higher than that in the first cycle, probably due to the improved kinetics of the rGO/cobalt sulfide anode resulting from a microstructure alteration after the first lithiation process. This phenomenon commonly appears in other conversion reaction-based anode materials [45, 46]. The main oxidation peak at about 2.07 V could be ascribed to the oxidation of Co^0 to Co ion in the delithiation process. The CV curves of rGO/cobalt sulfide composite are almost overlapped after the 1st cycle, and show high symmetry shapes, indicating the reversible electrochemical reactions of the composite [28]. Furthermore, the microstructure alteration of the prepared composite after the first cycle is characterized by XRD. As shown in Fig. S5, no peaks except Cu substrate are observed after the first cycle, indicating the microstructure was totally changed at low potentials. This phenomenon is in good agreement with that of CoS_2 anode material [47]. EIS curves of the electrodes for the as-prepared composite and the pure cobalt sulfide were shown in Fig. 3b. It can be seen that each of the Nyquist plots consists of a depressed semicircle in the medium-frequency region and a linear part in the low-frequency region. The semicircle is attributed to the charge-transfer reaction at

the electrolyte/electrode interface. The subsequent straight line represents typical Warburg resistance, which is attributed to the diffusion of lithium ions in the bulk of the active anode materials. Clearly, the diameter of the semicircle of the rGO/cobalt sulfide composite electrode is much smaller than that of the pure cobalt sulfide, which means a higher electrochemical activity of the rGO/cobalt sulfide composite electrode, resulting in high capacity and good rate capability [24]. The decrease of resistance might be attributed to the high conductivity of the rGO.

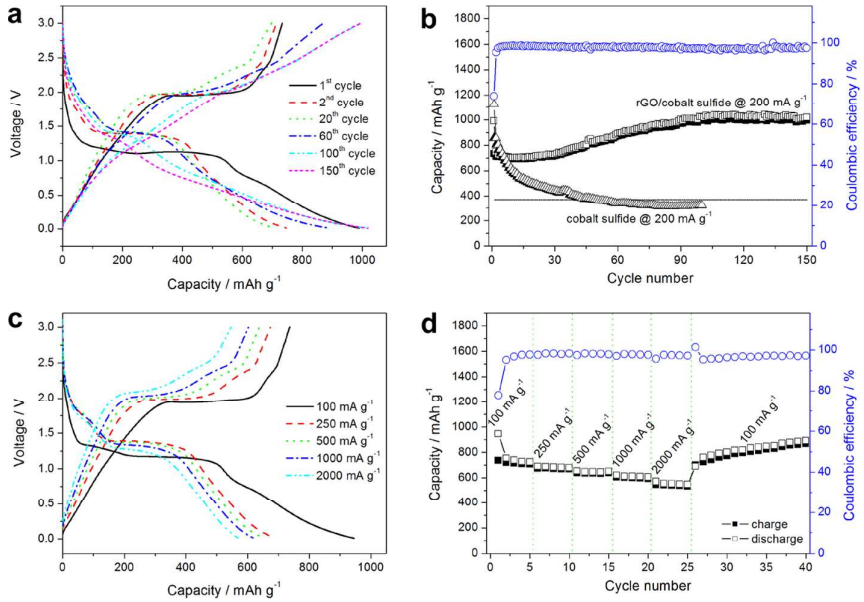

Fig. 4. (a) Discharge and charge voltage profiles of the rGO/cobalt sulfide composite, (b) Cycling performance of the prepared pure cobalt sulfide and rGO/cobalt sulfide electrode cycled at a current density of 200 mA g^{-1}, and corresponding Coulombic efficiency of rGO/cobalt sulfide electrode, (c) and (d) Rate-capability performance of the rGO/cobalt sulfide composite at various current densities of 100, 250, 500, 1000, and 2000 mA g^{-1}.

Performance of the as-prepared rGO/cobalt sulfide composite in battery was further studied by using a galvanostatic discharge/charge technique. Fig. 4a shows the 1st to 150th discharge/charge cycle of the composite at a current density of 200 mA g^{-1} over a voltage window of 0.01-3.0 V (vs. Li^+/Li). The initial discharge and reversible charge capacities of the composite anode are 990 and 733 mAh g^{-1}, respectively. The initial Coulombic efficiency is about 74%, comparable to or even higher than those of recently reported cobalt-based composites [24, 28-30]. The irreversible capacity loss in the 1st cycle is attributed to the electrolyte decomposition and the formation of solid electrolyte interface (SEI) film on the surface of electrode. During the 2nd cycle, the discharge capacity decreases to 748 mAh g^{-1} with a corresponding charge capacity of 713 mAh g^{-1}, showing a much higher Coulombic efficiency than the 1st cycle. Fig. 4b shows cycling stability of the pure cobalt sulfide and rGO/cobalt sulfide composite at a current density of 200 mA g^{-1}. After 150 discharge/charge cycles, the composite anode shows a high reversible capacity of 994 mAh g^{-1} with a Coulombic efficiency over 97%. This capacity value is even higher than the initial discharge capacity, and is much higher than that of the control battery using a pure cobalt sulfide anode (320 mAh g^{-1} after 100 cycles). Notably, this reversible capacity is higher than the theoretical capacity of cobalt sulfide (Co_9S_8: 539 mAh g^{-1}). Such a high reversible capacity indicates high accessibility for lithium ion insertion and extraction in this material and the excess over the theoretical value probably arises from interfacial lithium storage on the composite surfaces [45]. The good cycling performance might be ascribed to the homogeneous integration of the cobalt sulfide with the elastic rGO,

which can effectively accommodate the physical strains caused by the large volume changes during the charge/discharge process [48]. It should be noted that the capacity increases continuously as increasing the cycling numbers. The increased capacity could be attributed to the destruction in the graphite lattice during the lithiation/delithiation and the generation of more defects and active sites for lithium ion storage [49, 50] and the reversible growth of the polymeric gel-like film by the kinetically activated electrolyte degradation, which has also been observed in previous literatures [28, 51, 52].

Good rate performances are desirable for developing LIBs with high power densities. The rate capability of the as-prepared composite was evaluated at various current densities. Figs. 4c and d show the rate capability of the prepared composite over a voltage window of 0.01-3.0 V. The discharge capacities are about 724, 678, 651, 607, and 547 mAh g^{-1} at the current densities of 100, 250, 500, 1000, and 2000 mA g^{-1}, respectively. Up to 76% discharge capacity is retained from 100 mA g^{-1} to 2000 mA g^{-1}. Moreover, after changing the current density from 2000 mA g^{-1} to 100 mA g^{-1}, the discharge capacity first recovers to 690 mAh g^{-1} and increases to 868 mAh g^{-1} after another 40 discharge/charge cycles, showing its excellent reversibility. In contrast, the pure cobalt sulfide exhibits much worse rate performance (560 mAh g^{-1} after 30 cycles, Fig. S6 in Supporting Information). For the conversion reaction-based materials, the poor cycling stability has always been a bottleneck for practical application. Compared with the recent studies on LIB with cobalt sulfide/graphene composite anodes (Table S1 in Supporting Information), the composite in this work

possesses good capacity retention and a high capacity. The improvement in electrochemical Li-ion storage performance of the as-prepared rGO/cobalt sulfide composite is attributed to the following factors: i) the thin particle-sheet structure of the rGO/cobalt sulfide electrode which greatly decrease the inter-particle resistance of electron pathways, shortens the diffusion length for both electrons and Li ions, and facilitates the transport of electrons in the bulk electrode during the discharging/charging; and ii) the elastic rGO matrix not only acts as the support for cobalt sulfide and provides high electrical conductivity pathway, but also accommodates the volume changes and prevents the breakdown of the overall electrode during the cycling process [53, 54].

4. Conclusions

In summary, we have developed a simple but efficient ultrasonic-assisted wet chemical method to fabricate uniform cobalt sulfide nanocrystals on rGO. The as-prepared rGO/cobalt sulfide composite shows much better electrochemical performance including higher reversible capacity and rate capacity than pure cobalt sulfide material in LIB applications. The improvements in capacity, cycling stability and rate capability can be attributed to the synergetic effect between the small cobalt sulfide nanoparticles and conductive rGO matrix. It is envisaged that the present method may be adaptable for the large-scale production of metal sulfide/rGO composites for next generation energy transfer and storage device applications.

References

[1] A.S. Arico, P. Bruce, B. Scrosati, J.-M. Tarascon, W. van Schalkwijk, Nanostructured materials for advanced energy conversion and storage devices, Nat. Mater. 4 (2005) 366.

[2] J. B. Goodenough, Y. Kim, Challenges for rechargeable Li batteries, Chem. Mater. 22 (2010) 587.

[3] M. Armand, J. M. Tarascon, Building better batteries, Nature 451 (2008) 652.

[4] N. Mahmood, C. Zhang, Y. Hou, Nickel sulfide/nitrogen-doped graphene composites: Phase-controlled synthesis and high performance anode materials for lithium ion batteries, Small 9 (2013) 1321.

[5] C. He, S. Wu, N. Zhao, C. Shi, E. Liu, J. Li, Carbon-encapsulated Fe_3O_4 nanoparticles as a high-rate lithium ion battery anode material, ACS Nano 7 (2013) 4459.

[6] J.M. Jeong, B.G. Choi, S.C. Lee, K.G. Lee, S.-J. Chang, Y.K. Han, Y.B. Lee, H.U. Lee, S. Kwon, G. Lee, C.-S. Lee, Y.S. Huh, Hierarchical hollow spheres of Fe_2O_3@polyaniline for lithium ion battery anodes, Adv. Mater. 25 (2013) 6250.

[7] X. Zhou, L.J. Wan, Y.G. Guo, Binding SnO_2 nanocrystals in nitrogen-doped graphene sheets as anode materials for lithium-ion batteries, Adv. Mater. 25 (2013) 2152.

[8] S. Yang, G. Cui, S. Pang, Q. Cao, U. Kolb, X. Feng, J. Maier, K. Müllen, Fabrication of cobalt and cobalt oxide/graphene composites: Towards high-performance anode materials for lithium ion batteries. ChemSusChem 3 (2010) 236.

[9] G.M. Zhou, D.W. Wang, F. Li, L.L. Zhang, N. Li, Z.S. Wu, L. Wen, G.Q. Lu, H.M. Cheng, Graphene-wrapped Fe_3O_4 anode material with improved reversible capacity and cyclic stability for lithium ion batteries, Chem. Mater. 22 (2010) 5306.

[10] F. Gillot, J. Oró-Solé, M.R. Palacín, Nickel nitride as negative electrode material for lithium ion batteries, J. Mater. Chem. 21 (2011) 9997.

[11] L. Baggetto, N.A.M. Verhaegh, R.A.H. Niessen, F. Roozeboom, J.-C. Jumas, P.H.L. Notten, Tin nitride thin films as negative electrode material for lithium-ion solid-state batteries, J. Electrochem. Soc. 157 (2010) A340.

[12] X. Jiang, X. Yang, Y. Zhu, J. Shen, K. Fan, C. Li, In situ assembly of graphene sheets-supported SnS_2 nanoplates into 3D macroporous aerogels for high-performance lithium ion batteries, J. Power Sources 237 (2013) 178.

[13] B. Wu, H. Song, J. Zhou, X. Chen, Iron sulfide-embedded carbon microsphere anode material with high-rate performance for lithium-ion batteries, Chem. Commun. 47 (2011) 8653.

[14] N. Du, H. Zhang, J. Chen, J. Sun, B. Chen, D. Yang, Metal oxide and sulfide hollow spheres: Layer-by-layer synthesis and their application in lithium-ion battery, J. Phys. Chem. B 112 (2008) 14836.

[15] K. Chang, W. Chen, L-cysteine-assisted synthesis of layered MoS_2/graphene composites with excellent electrochemical performances for lithium ion batteries, ACS Nano 5 (2011) 4720.

[16] Y. Wang, J. Wu, Y. Tang, X. Lü, C. Yang, M. Qin, F. Huang, X. Li, X. Zhang,

Phase-controlled synthesis of cobalt sulfides for lithium ion batteries, ACS Appl. Mater. Interfaces 4 (2012) 4246.

[17] J.M. Yan, H.Z. Huang, J. Zhang, Z.J. Liu, Y. Yang, A study of novel anode material CoS_2 for lithium ion battery, J. Power Sources 146 (2005) 264.

[18] Y.X. Zhou, H.B. Yao, Y. Wang, H.L. Liu, M.R. Gao, P.K. Shen, S.H. Yu, Hierarchical hollow Co_9S_8 microspheres: Solvothermal synthesis, magnetic, electrochemical, and electrocatalytic properties, Chem. Eur. J. 16 (2010) 12000.

[19] C. Wang, Y. Zhou, M. Ge, X. Xu, Z. Zhang, J.Z. Jiang, Large-scale synthesis of SnO_2 nanosheets with high lithium storage capacity, J. Am. Chem. Soc. 132 (2010) 46.

[20] J. Lin, Z. Peng, C. Xiang, G. Ruan, Z. Yan, D. Natelson, J.M. Tour, Graphene nanoribbon and nanostructured SnO_2 composite anodes for lithium ion batteries, ACS Nano 7 (2013) 6001.

[21] M.S. Park, G.X. Wang, Y.M. Kang, D. Wexler, S.X. Dou, H.K. Liu, Preparation and electrochemical properties of SnO_2 nanowires for application in lithium-ion batteries, Angew. Chem. Int. Ed. 46 (2007) 750.

[22] S. Ko, J.I. Lee, H.S. Yang, S. Park, U. Jeong, Mesoporous CuO particles threaded with CNTs for high-performance lithium-ion battery anodes, Adv. Mater. 24 (2012) 4451.

[23] J.S. Chen, X.W. Lou, SnO_2-based nanomaterials: Synthesis and application in lithium-ion batteries, Small 9 (2013) 1877.

[24] W. Shi, J. Zhu, X. Rui, X. Cao, C. Chen, H. Zhang, H.H. Hng, Q. Yan, Controlled

synthesis of carbon-coated cobalt sulfide nanostructures in oil phase with enhanced Li storage performances, ACS Appl. Mater. Interfaces 4 (2012) 2999.

[25] Z. Wang, J. Liu, W. Wang, H. Chen, Z. Liu, Q. Yu, H. Zeng, L. Sun, Aqueous phase preparation of graphene with low defect density and adjustable layer, Chem. Commun. 49 (2013) 10835.

[26] X. Zhu, Y. Zhu, S. Murali, M.D. Stoller, R.S. Ruoff, Nanostructured reduced graphene oxide/Fe_2O_3 composite as a high-performance anode material for lithium ion batteries, ACS Nano 5 (2011) 3333.

[27] H. Wang, L.F. Cui, Y. Yang, H.S. Casalongue, J.T. Robinson, Y. Liang, Y. Cui, H. Dai, Mn_3O_4-graphene hybrid as a high-capacity anode material for lithium ion batteries, J. Am. Chem. Soc. 132 (2010) 13978.

[28] J. Xie, S. Liu, G. Cao, T. Zhu, X. Zhao, Self-assembly of CoS_2/graphene nanoarchitecture by a facile one-pot route and its improved electrochemical Li-storage properties, Nano Energy 2 (2013) 49.

[29] G. Huang, T. Chen, Z. Wang, K. Chang, W. Chen, Synthesis and electrochemical performances of cobalt sulfides/graphene nanocomposite as anode material of Li-ion battery, J. Power Sources 235 (2013) 122.

[30] N. Mahmood, C. Zhang, J. Jiang, F. Liu, Y. Hou, Multifunctional Co_3S_4/graphene composites for lithium ion batteries and oxygen reduction reaction, Chem. Eur. J. 19 (2013) 5183.

[31] Y. Gu, Y. Xu, Y. Wang, Graphene-wrapped CoS nanoparticles for high-capacity lithium-ion storage, ACS Appl. Mater. Interfaces 5 (2013) 801.

[32] W.S. Hummers, R.E. Offeman, Preparation of graphitic oxide, J. Am. Chem. Soc. 80 (1958) 1339.

[33] N.I. Kovtyukhova, P.J. Ollivier, B.R. Martin, T.E. Mallouk, S.A. Chizhik, E.V. Buzaneva, A.D. Gorchinskiy, Layer-by-layer assembly of ultrathin composite films from micron-sized graphite oxide sheets and polycations, Chem. Mater. 11 (1999) 771.

[34] Z. Li, J. Wang, S. Liu, X. Liu, S. Yang, Synthesis of hydrothermally reduced graphene/MnO_2 composites and their electrochemical properties as supercapacitors, J. Power Sources 196 (2011) 8160-8165.

[35] X. Xia, C. Zhu, J. Luo, Z. Zeng, C. Guan, C.F. Ng, H. Zhang, H.J. Fan, Synthesis of free-standing metal sulfide nanoarrays via anion exchange reaction and their electrochemical energy storage application, Small 10 (2014) 766.

[36] Q. Liu, J. Zhang, A general and controllable synthesis of Co_mS_n (Co_9S_8, Co_3S_4, and $Co_{1-x}S$) hierarchical microspheres with homogeneous phases, CrystEngComm 15 (2013) 5087.

[37] C. Loussot, P. Afanasiev, M. Vrinat, H. Jobic, P.C. Leverd, Amorphous cobalt oxysulfide as a hydrogen trap, Chem. Mater. 18 (2006) 5659.

[38] Z. Wang, L. Pan, H. Hu, S. Zhao, Co_9S_8 nanotubes synthesized on the basis of nanoscale Kirkendall effect and their magnetic and electrochemical properties, CrystEngComm 12 (2010) 1899.

[39] Q. Wang, L. Jiao, H. Du, Y. Si, Y. Wang, H. Yuan, Co_3S_4 hollow nanospheres grown on graphene as advanced electrode materials for supercapacitors, J. Mater.

Chem. 22 (2012) 21387.

[40] K. Polychronopoulou, C.D. Malliakas, J. He, M.G. Kanatzidis, Selective surfaces: Quaternary Co(Ni)MoS-based chalcogels with divalent (Pb^{2+}, Cd^{2+}, Pd^{2+}) and trivalent (Cr^{3+}, Bi^{3+}) metals for gas separation, Chem. Mater. 24 (2012) 3380.

[41] S. Zhao, Y. Peng, The oxidation of copper sulfide minerals during grinding and their interactions with clay particles, Powder Technol. 230 (2012) 112.

[42] V.N. Bui, D. Laurenti, P. Delichère, C. Geantet, Hydrodeoxygenation of guaiacol Part II: Support effect for CoMoS catalysts on HDO activity and selectivity, Appl. Catal. B: Environ. 101 (2011) 246.

[43] H.S. Kim, T.S. Arthur, G.D. Allred, J. Zajicek, J.G. Newman, A.E. Rodnyansky, A.G. Oliver, W.C. Boggess, J. Muldoon, Structure and compatibility of a magnesium electrolyte with a sulphur cathode, Nat. Commun. 2 (2011) 427.

[44] J.L. Gómez-Cámer, F. Martin, J. Morales, L. Sánchez, Precipitation of CoS vs ceramic synthesis for improved performance in lithium cells, J. Electrochem. Soc. 155 (2008) A189.

[45] Y. Sun, X. Hu, W. Luo, F. Xia, Y. Huang, Reconstruction of conformal nanoscale MnO on graphene as a high-capacity and long-life anode material for lithium ion batteries, Adv. Funct. Mater. 23 (2013) 2436.

[46] O. Delmer, P. Balaya, L. Kienle, J. Maier, Enhanced potential of amorphous electrode materials: Case study of RuO_2, Adv. Mater. 20 (2008) 501.

[47] J.M. Yan, H.Z. Huang, J. Zhang, Z.J. Liu, Y. Yang, A study of novel anode material CoS_2 for lithium ion battery, J. Power Sources 146 (2005) 264.

[48] X. Huang, R. Wang, D. Xu, Z. Wang, H. Wang, J. Xu, Z. Wu, Q. Liu, Y. Zhang, X. Zhang, Homogeneous CoO on graphene for binder-free and ultralong-life lithium ion batteries, Adv. Funct. Mater. 23 (2013) 4345.

[49] J. Zhu, Y. Li, S. Kang, X.-L. Wei, P. K. Shen, One-step synthesis of Ni_3S_2 nanoparticles wrapped with in situ generated nitrogen-self-doped graphene sheets with highly improved electrochemical properties in Li-ion batteries, J. Mater. Chem. A 2 (2014) 3142.

[50] K. Chang, D. Geng, X. Li, J. Yang, Y. Tang, M. Cai, R. Li, X. Sun, Ultrathin MoS_2/nitrogen-doped graphene nanosheets with highly reversible lithium storage, Adv. Energy Mater. 3 (2013) 839.

[51] G. M. Zhou, D. W. Wang, F. Li, L. L. Zhang, N. Li, Z. S. Wu, L. Wen, G. Q. Lu, H. M. Cheng, Graphene-wrapped Fe_3O_4 anode material with improved reversible capacity and cyclic stability for lithium ion batteries, Chem. Mater. 22 (2010) 5306.

[52] W. Wei, S. Yang, H. Zhou, I. Lieberwirth, X. Feng, K. Müllen, 3D graphene foams cross-linked with pre-encapsulated Fe_3O_4 nanospheres for enhanced lithium storage, Adv. Mater. 25 (2013) 2909.

[53] Y. Huang, D. Wu, S. Han, S. Li, L. Xiao, F. Zhang, X. Feng, Assembly of tin oxide/graphene nanosheets into 3D hierarchical frameworks for high-performance lithium storage, ChemSusChem 6 (2013) 1510.

[54] D. Wang, J. Yang, X. Li, D. Geng, R. Li, M. Cai, T.-K. Sham, X. Sun, Layer by layer assembly of sandwiched graphene/SnO_2 nanorod/carbon nanostructures

with ultrahigh lithium ion storage properties, Energy Environ. Sci. 6 (2013) 2900.

Facile fabrication and electrochemical properties of high-quality reduced graphene oxide/cobalt sulfide composite as anode material for lithium-ion batteries

Zhangpeng Li,[a] Wenyue Li,[a,b] Hongtao Xue,[a] Wenpei Kang,[a] Xia Yang,[a] Mingliang Sun,[a] Yongbing Tang*[a,b] and Chun-Sing Lee*[a]

[a] Center of Super-Diamond and Advanced Films (COSDAF), Department of Physics and Materials Science, City University of Hong Kong, Kowloon, Hong Kong SAR, People's Republic of China.

[b] Functional Thin Films Research Center, Shenzhen Institutes of Advanced Technology, Chinese Academy of Sciences, Shenzhen, People's Republic of China.

E-mail: ybtang@cityu.edu.hk; apcslee@cityu.edu.hk; Tel: +852-34427826

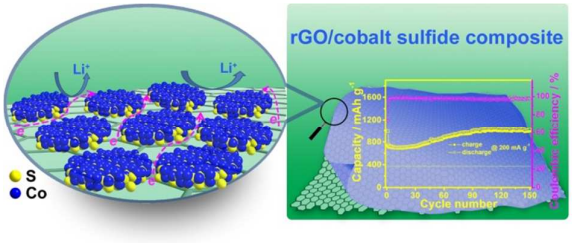

A simple and efficient ultrasound-assisted wet chemical-synthesized rGO/cobalt sulfide anode exhibits high lithium storage capacity and excellent rate capability.